Intrinsic Frequency Response of Silicon–Germanium Phototransistor Associated With 850-nm Multimode Fiber

Zerihun Gedeb Tegegne, Carlos Viana, Jean-Luc Polleux, Marjorie Grzeskowiak, and Elodie Richalot

***Abstract*— The intrinsic frequency response of silicon–germanium heterojunction bipolar phototransistors (HPTs) at 850 nm is studied to be implemented in multimode fiber systems. The experimental analysis of an HPT with an optical window size of 10 × 10 μm^2 is presented. An opto-microwave (OM) scanning near-field optical microscopy is performed to observe the variation of the HPT dynamic behavior versus the illumination location of the phototransistor. The photocurrent generated by the photodiode at the interface between the n^{++} subcollector and the p^+ guard ring is analyzed, and its impact on the performance of the HPT is investigated. Then, we propose a technique to remove the substrate photocurrent effect on the optical transition frequency (f_{Topt}): f_{Topt} value of 4.1 GHz given by raw measurement results increases up to 6 GHz after removing the substrate response. The influence of the 2-D carrier flows on the HPT intrinsic OM behavior is also studied. Design aspects of SiGe/Si HPT structures are finally discussed as a conclusion.**

***Index Terms*— Microwave photonics, opto-microwave scanning near-field optical microscopy (OM-SNOM), silicon-based photodetectors, SiGe phototransistor, substrate effect.**

I. Introduction

AN INTEREST has been recently developed in the implementation of SiGe heterojunction bipolar phototransistors (HPTs) into radio-over-fiber home area network [1], [2], for which low-cost optoelectronic devices at 850 nm are in demand. HPTs can also be specifically used in nonlinear circuits such as direct optical injection-locked oscillator and self-mixers [3], [4]. From 1997 to 2000, multiple-quantum-well SiGe/Si HPT was proposed [5], [6]; however, these components are not directly implementable in commercial SiGe BiCMOS technological processes used for electronic parts. Single-layer SiGe HPTs have been developed since 2003 [7]–[10] based on a standard SiGe heterojunction bipolar transistor (HBT) technology. Recently, SiGe HPTs were successfully implemented in the transmission chain of 3-Gb/s IEEE 802.11.3c signals [1].

There is a continuous interest to develop phototransistors from newer standard SiGe HBT technologies that offer faster operating frequencies to improve the performances of the HPTs without modifying the vertical stack of layers imposed by the technological process. To optimize the phototransistor speed, Moutier *et al.* [11] performed physical simulations to observe the fastest and slowest regions of HPTs' structure. Helme and Houstron [12] and Yuan *et al.* [13] investigated the phototransistor performances through optoelectronic compact circuit modeling. The existence of substrate photocurrent was demonstrated in [13]–[15].

This paper develops a mathematical procedure to remove the substrate response and to extract the core performances of SiGe HPT such as the optical transition frequency (f_{Topt}). Concerning these core performances, the intrinsic electrical parameters such as the junction capacitance and transient time are deduced, and then the influence of the 2-D carrier flow (near the metal contacts) on the device speed is demonstrated. A conclusion is then drawn on the design aspects of SiGe/Si HPTs to improve their performances. The measurement of the phototransistor frequency characteristics is performed under multimode optical fiber illumination. While measurement under single-mode fiber illumination would bring clear information on the physics of the device, it is also essential to include the impact of the distribution of the multimode fiber (MMF) optical beam on such characteristics with a view to commercial implementation.

II. SiGe/Si HPT Structure and Technology

The SiGe HPT is fabricated using the conventional SiGe2RF Telefunken GmbH process for bipolar SiGe transistors. Indeed, the phototransistor fabrication respects the vertical stack of layers used in the standard SiGe2RF HBT technology. This guarantees the compatibility with this technological process and enables the potential integration of photonic and electronic circuits.

The phototransistor is designed by extending the emitter, base, and collector layers of the reference HBT [15]. The optical injection is made vertically through the emitter. A cross section of the phototransistor structure is given in Fig. 1. The light path goes through the oxide and polysilicon of the emitter before entering the Si emitter, SiGe base, and Si collector

The authors are with the ESYCOM (EA2552), ESIEE-Paris, UPEM, Le CNAM, Université Paris-Est, 93162 Noisy-le-Grand, France (e-mail: ztzerihun0@gmail.com; jl.polleux@esiee.fr).

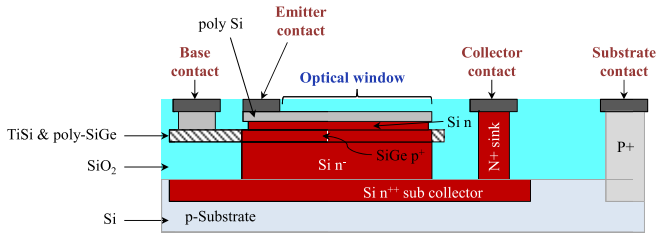

Fig. 1. Simplified schematic cross section of HPT with extended emitter, base, and collector regions.

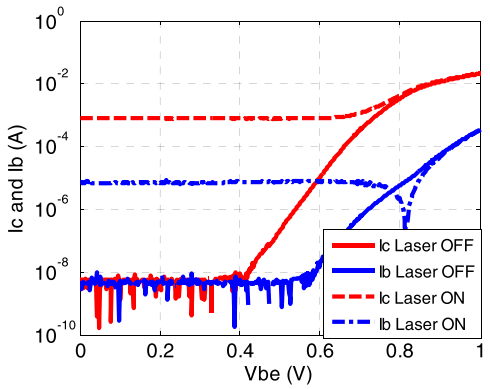

Fig. 2. Gummel plot under 2.28-mW optical power illumination and dark conditions.

regions. This HPT is essentially one large HBT whose emitter metallization only partially covers the emitter region. The substrate is grounded through a p^+ guard ring around the HPT.

We have designed phototransistors with a 10×10 μm^2 optical opening. The base region consists of a 40–80-nm-thin SiGe layer with Ge content of 20%–25% and high p doping in the range of 10^{19} cm^{-3} as presented in [6]. The collector is typically 300–400 nm thick with low doping and the emitter region is less than 100 nm thick. The doping levels of each region are estimated in [16].

III. Experimental Results and Discussion

A. Substrate Photodiode Current Analysis

The Gummel plots under illumination (at 850-nm wavelength) and dark conditions are shown in Fig. 2. The current at low base–emitter voltage (V_{be}) corresponds to the photocurrent which is far lower than the current induced by the transistor effect observed at higher base–emitter voltage. Under illumination condition, the base current in Fig. 2 is represented by its absolute value. At low V_{be}, base current I_b has a negative sign and hence flows out of the base contact. Its sign changes at $V_{be} = 0.82$ V, where its amplitude is minimal.

Under dark condition and at low V_{be}, the magnitude of collector current I_c and base current I_b are equal, whereas for the same biasing condition with the light "ON," the magnitude of I_c and I_b are different. This behavior is not encountered with phototransistors such as InGaAs/InP HPTs [17] (for which the magnitude of I_b and I_c are equal at low base–emitter voltage and under illumination condition), where the InP substrate is optically transparent at the wavelength of interest. As indicated in Fig. 3, the holes (h^+) generated in

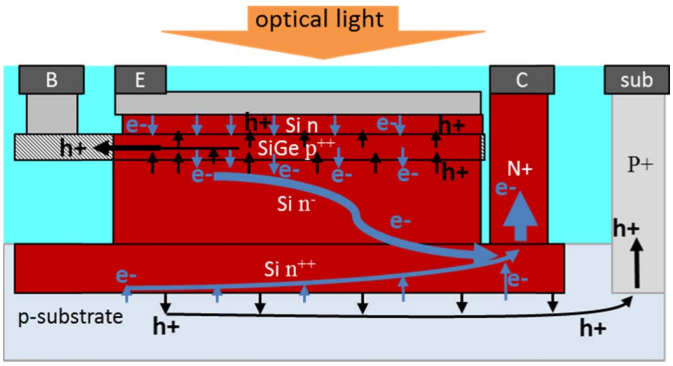

Fig. 3. Schematic that indicates the flow of photogenerated carriers that are generated at different regions of the HPT.

the substrate diode are effetely grounded via the substrate contact. However, the electrons (e^-) generated in the substrate diode are combined with the electrons which are generated in the active region (emitter–base–collector) of the HPT to reach the collector contact and measured as collector current I_C. When V_{be} is greater than 0.7 V, most parts of the holes generated at the base–collector junction attract electrons from the emitter for transistor amplification and some parts are, however, escaped to the base contact, whereas, when V_{be}less than 0.4 V, all photogenerated holes generated within the active region are flowing out into the base contact and can be measured as base current I_b. Thus, the difference between the collector and base photocurrent magnitudes shown in Fig. 2 at $V_{be} = 0$ V corresponds to the photocurrent generated by the substrate diode called substrate photocurrent (I_{sub}) [14]. This can be computed using the following equation:

$$I_{sub} = (I_{C,PD} - I_{C,PD,dark}) - (I_{b\_PD} - I_{b\_PD\_dark}) \quad (1)$$

where $I_{b\_PD_{dark}}$ and $I_{C,PD,dark}$ are, respectively, the dark base and collector currents in photodiode (PD) mode (at $V_{be} = 0$ V). $I_{C,PD}$ and $I_{b,PD}$ are the collector and base currents under illumination condition.

To locate the source of this extra photocurrent in the phototransistor structure and to study its impact on the opto-microwave (OM) behavior of the HPT, we performed a dc and an OM mapping of the devices using scanning near-field optical microscopy (SNOM) with the measurement setup described in [18] and [19], where a 850-nm vertical cavity surface emitting laser (of 12-GHz cutoff frequency) is directly modulated to illuminate the HPT through a lensed MMF moved over the HPT surface.

Fig. 4(a) shows the microscopic photography of a 10×10 μm^2 phototransistor (over which the topological mapping is performed), where the ground (emitter contact) and signal (base and collector) lines are clearly visible. The base contact is taken from the left side, collector contact from the right side, and the emitter contact is connected at its top and bottom sides to the ground (common emitter configuration). The layout is accordingly sketched in Fig. 4(b), which defines the coordinates of the optical fiber center; its origin is fixed at the center of the optical window.

We performed the experimental mapping (consisting of displacing the illuminating optical fiber) on HPT at two

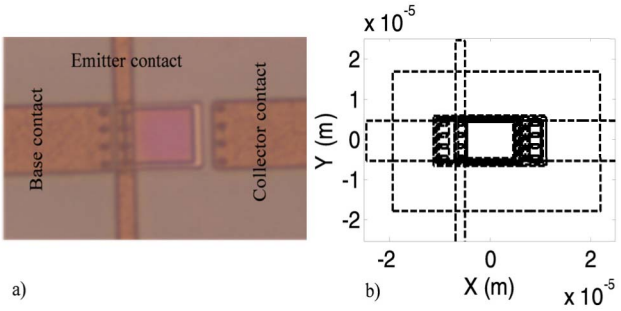

Fig. 4. (a) Top view of the phototransistor. (b) Layout of a 10 × 10 μm^2 optical window phototransistor and optical fiber coordinate axes centered at the center of optical window.

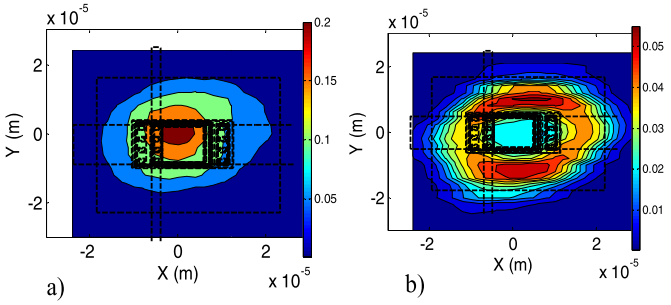

Fig. 5. Low-frequency (50 MHz) OM responsivity of HPT with 10 × 10 μm^2 in (a) HPT mode ($V_{be} = 0.857$ V) and (b) PD mode ($V_{be} = 0$ V) for $V_{ce} = 3$ V loaded by 50 Ω.

different bias conditions, i.e., at $V_{be} = 0$ V and $V_{be} = 0.857$ V for $V_{ce} = 3$ V. The phototransistor mode (HPT mode) is obtained by fixing the collector–emitter voltage at 3 V and a fixed base–emitter voltage at 0.857 V. These biasing conditions correspond to the optimal ones in terms of OM responsivity. In this mode, there is an internal amplification of photogenerated carriers due to transistor effect (current gain β). The PD mode (PD mode) is obtained by setting the collector–emitter voltage at 3 V and the base–emitter voltage at 0 V. In PD mode, as the base–emitter junction is electrically inactive, there is no amplification in the device so that the purely photogenerated currents can be extracted. The dc current and OM frequency response of the HPT is then measured at each location of the illuminating optical beam in both modes. An injected optical power level of 2.38 mW is used in the subsequent experimental results.

B. Substrate Photocurrent Effect on Opto-Microwave Behavior

The OM power gain represents the ratio of the HPT microwave output signal power to the output power of a PD with 1 A/W responsivity [5]. It is equal to the square of the responsivity under 50-Ω load condition but may change as a function of the load as described in depth in [20]. OM gain is extracted from the S-parameter measurement as a function of frequency. Fig. 5(a) and (b) shows the low-frequency (50 MHz) OM responsivity of a 10×10 μm^2 optical window size HPT (loaded by 50 Ω) as a function of the optical fiber position in HPT and PD modes, respectively. In HPT mode, the peak of the responsivity appears inside the optical window, whereas in PD mode, the responsivity is maximal when the optical fiber is around the optical window according to a ring shape, as shown in Fig. 5(b).

The ring shape of the maximal responsivity in PD mode is due to the illumination of the substrate diode; we can observe the responsivity of the substrate diode is clearly stronger than the one of the PD created by the base and collector in the active region. As shown in Fig. 5(a), the ring shape does not appear in phototransistor mode as the substrate diode effect is hidden by the transistor amplification.

Fig. 6 presents the OM gain (Gom) as a function of the frequency at different optical fiber locations extracted from Fig. 5(b) (in PD mode). The Gom at $X = 2$ μm and

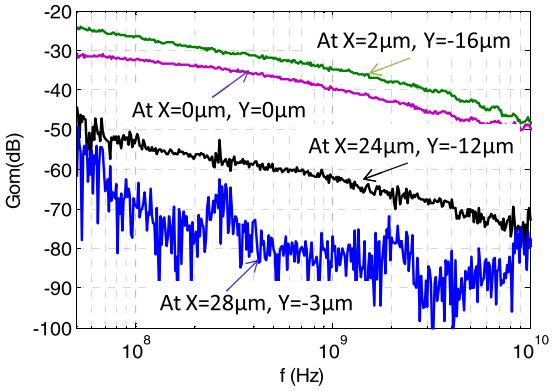

Fig. 6. Gom as a function of frequency in PD mode at different positions of optical fiber extracted from Fig. 9(b).

$Y = -16$ μm (outside the optical window) is higher than the Gom at the center ($X = Y = 0$ μm) at all frequencies. From this result, we can deduce that the substrate diode is clearly dominating over the intrinsic diode (the diode created by the base and collector) even at the central position despite the optical beam is attenuated by the layer vertical stack. When the optical fiber moves further away from the optical window, the low-frequency Gom decreases until reaching the noise level as the substrate diode becomes slower and then noneffective to detect the 50-MHz signal. The Gom curves at ($X = 24$ μm and $Y = -12$ μm) and ($X = 28$ μm and $Y = -3$ μm) illustrate this evolution in Fig. 6.

The substrate responsivity can be isolated from the intrinsic behavior by the mathematical model. The PD-mode intrinsic responsivity ($R_{PD,i}$), substrate responsivity (R_{sub}), and raw responsivity ($R_{om,PD}$) for an illuminated beam displacing along the y-axis ($X = 0$) are presented in Fig. 7. Indeed, $R_{om,PD}$ curve corresponds to the variation along the line $X = 0$ of the PD-mode responsivity measured at 50 MHz and presented in Fig. 5(b). To extract the substrate responsivity at 50 MHz, we use the definition of OM power gain in [7], and considering the 50-Ω load, it becomes

$$G_{om} = \frac{\frac{1}{2}R_0(I_{c,PD})^2}{\frac{1}{2}R_0(I_{opt,RF})^2} = R_{om,PD}^2 \Rightarrow \text{ with } I_{opt,RF} = \alpha_{cal} P_{opt,RF} \quad (2)$$

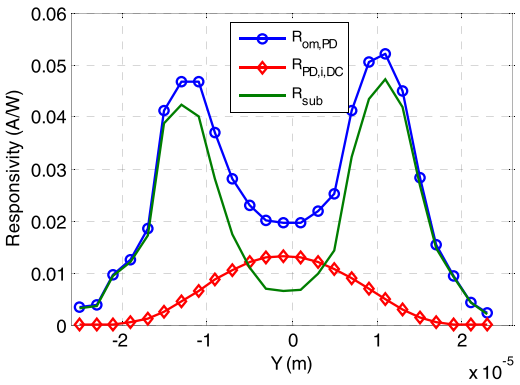

Fig. 7. Raw ($R_{\text{om,PD}}$), substrate (R_{sub}), and intrinsic responsivity ($R_{\text{PD},i,\text{dc}}$) of HPT with a 10×10 μm^2 optical window size in PD-mode operation ($V_{\text{be}} = 0$ V) and for an optical beam along the y-axis ($X = 0$).

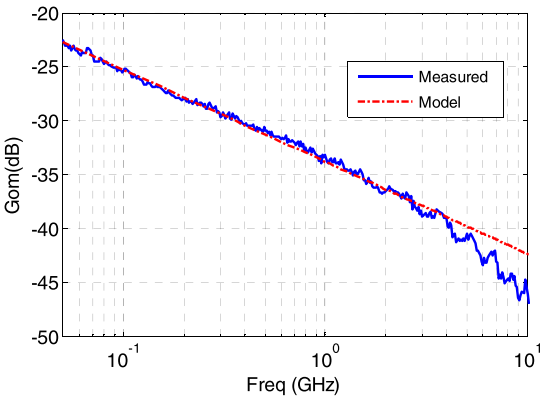

Fig. 8. Transfer function model fit to the measured OM gain of the substrate PD (optical fiber located at $X = 5$ μm and $Y = 15$ μm, and biases $V_{\text{be}} = 0$ V and $V_{\text{ce}} = 3$ V). The level of the injected optical power is 2.38 mW.

and

$$I_{C,\text{PD}} = I_{C,\text{PD,ph}} + I_{C,\text{PD,dark}} + I_{\text{sub}} \tag{3}$$

where $I_{C,\text{PD}}$ is the total current measured at the collector contact in PD mode, $I_{C,\text{PD,ph}}$ is the photocurrent generated in the HPT active area in PD mode, $I_{C,\text{PD,dark}}$ is the dark current measured at the collector contact, I_{sub} is the substrate photocurrent, $R_{\text{om,PD}}$ is the raw OM responsivity in PD mode, α_{cal} is a 1 A/W normalization factor, and $P_{\text{opt,RF}}$ is the illuminating optical power expressed as the equivalent current $I_{\text{opt,RF}}$. Then, we deduce the intrinsic responsivity

$$R_{\text{PD},i}^2 = \left(\frac{I_{C,\text{PD,ph}}}{I_{\text{opt,RF}}}\right)^2 = \left(\frac{I_{C,\text{PD}} - I_{C,\text{PD,dark}} - I_{\text{sub}}}{I_{\text{opt,RF}}}\right)^2 = \left(R_{\text{om,PD}} - R_{\text{sub}}\right)^2 \tag{4}$$

$$R_{\text{PD},i} = \frac{I_{C,\text{PD}} - I_{C,\text{PD,dark}}}{I_{\text{opt,RF}}} - \frac{I_{\text{sub}}}{I_{\text{opt,RF}}} = R_{\text{om,PD}} - R_{\text{sub}}. \tag{5}$$

To extract the substrate responsivity (R_{sub}) at low frequency, we assume that the intrinsic dc responsivity ($R_{\text{PD},i,\text{dc}}$) is equal to the intrinsic responsivity at low frequency ($R_{\text{PD},i,\text{LF}}$), this assumption being valid for $V_{\text{ce}} = 3$ V with no amplitude variation at low frequency. Hence,

$$R_{\text{PD},i,\text{LF}} = \frac{I_{C,\text{PD,ph}}}{I_{\text{opt,RF}}} \simeq \frac{I_{C,\text{PD,ph}}}{I_{\text{opt,DC}}} = R_{\text{PD},i,\text{DC}}. \tag{6}$$

Thus, the substrate responsivity (R_{sub}) at low frequency is calculated from (5) and (6)

$$R_{\text{sub}} = R_{\text{om,PD}} - R_{\text{PD},i,\text{LF}}. \tag{7}$$

As presented in Fig. 7, the peak of intrinsic responsivity ($R_{\text{PD},i,\text{dc}}$) appears at the center of the optical window ($X = Y = 0$ μm), whereas at the same location, the substrate PD responsivity is weaker than the intrinsic PD responsivity. However, the substrate response becomes stronger when the optical beam moves outside the optical window (around $Y = \pm 10$ μm). The substrate responsivity is low in HPT's active region, but it is not null due to the optical light penetration through the HPT to the substrate, underneath the active region.

The dynamic behavior of the phototransistor can be analyzed through the optical transition frequency (f_{Topt}). The latter is defined as the frequency at which the 50-Ω OM gain in HPT mode is equal to the 50-Ω low-frequency gain in PD mode ($V_{\text{be}} = 0$ V). Indeed, it is the frequency at which the phototransistor stops amplifying, as shown in Fig. 9.

As it has been demonstrated in [14], the substrate photocurrent in SiGe HPT has a huge impact on the frequency response of the phototransistor mainly in PD mode. To observe the intrinsic properties of the HPT (that can be used for future SiGe HPT modeling), one needs to remove (de-embed) the substrate response from the raw measured data at each position of the optical fiber and at all frequencies. The substrate response at low frequency computed by (7) is extrapolated to all frequencies using the transfer function presented in the following equation:

$$R_{\text{sub}}(f) = \frac{R_{\text{sub}}(f_0)}{\left(1 + j\frac{f}{f_0}\right)^{\alpha}} \tag{8}$$

where f_0 is 50 MHz, and $\propto$ is the order of the transfer function to model the frequency slope of the substrate PD.

Fig. 8 shows the fitting of the model with the experimental OM gain measured by illuminating the structure at $X = 5$ μm and $Y = 15$ μm, where the substrate photocurrent amplitude is maximum. The model well fits with the measurement results for $\propto = 0.4$ corresponding to an 8 dB/decay slope of Gom.

The substrate diode influence is then removed at all frequencies from the phototransistor responsivity to obtain the intrinsic responsivity in phototransistor mode ($R_{\text{HPT},i}$). The intrinsic optical transition frequency ($f_{\text{Topt,int}}$) is the frequency at which $R_{\text{HPT},i}$ is equal to the intrinsic dc responsivity in PD mode ($R_{\text{PD},i,\text{dc}}$).

The complete and intrinsic OM gains versus frequency in PD and HPT modes when the optical beam focuses at the center of the optical window ($X = 0$ μm and $Y = 0$ μm) are presented in Fig. 9. The model of substrate PD frequency response at $X = Y = 0$ μm is also presented in Fig. 9. The raw and intrinsic Gom are equal at all frequencies in the HPT mode operation. This indicates that the frequency response of the substrate PD is hidden by the internal transistor amplification effect. However, in PD mode, the substrate PD contributes to its OM gain and reduces its speed.

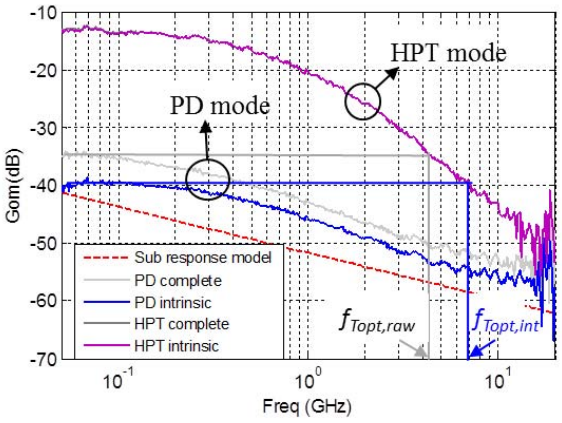

Fig. 9. OM gain in PD and phototransistor modes for an optical beam located at $X = 0$ μm and $Y = 0$ μm. The level of the injected optical power is 2.38 mW.

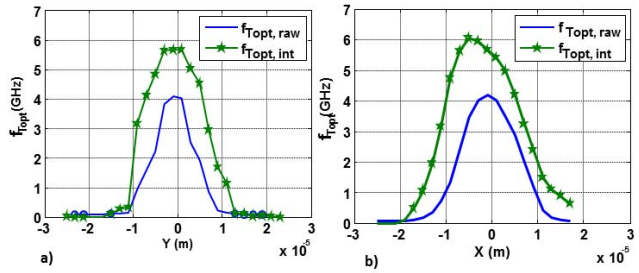

Fig. 10. Optical transition frequency before and after removing the substrate diode effect with the optical beam centered at (a) $X = 0$ μm and (b) $Y = 0$ μm.

The variation of f_{Topt} at $X = 0$ μm along the y-axis is shown in Fig. 10(a) before and after removing the substrate diode effect. The flat $f_{\text{Topt,int}}$ peak appears over the optical window (the peak width is about 10 μm), and it drops to 0 outside the optical window.

Whereas, along the x-axis, the intrinsic $f_{\text{Topt,int}}$ is not flat over the optical window [Fig. 10(b)], the intrinsic $f_{\text{Topt,int}}$ peak is shifted from the center of the optical window toward the base and emitter contacts. This is because when the optical beam is injected close to the base and emitter contacts, the distance traveled by the holes to reach the base and emitter contacts become very short, whereas when the optical beam is injected at the center of the optical window, the distance traveled by the holes to reach the base and emitter contacts is longer as the related transit time. The f_{Topt} peak is improved from 4.1 to 6 GHz while extracting substrate diode effect.

Fig. 11 shows the intrinsic optical transition frequencies $f_{\text{Topt,int}}$ versus collector current (I_C). The presented optical transition frequency has been measured after optimizing the optical fiber location to obtain the higher $f_{\text{Topt,int}}$. The maximal value of $f_{\text{Topt,int}}$ reaches 6.5 GHz, indicating that this HPT could be implemented in optical applications operating up to 6.5 GHz.

f_{Topt} versus I_C curve (Fig. 11) can be divided into three mean regions.

1) *Low Current Region:* In this region f_{Topt} quickly increases with the collector current due to the junction capacitance reduction as the dc supply increases.

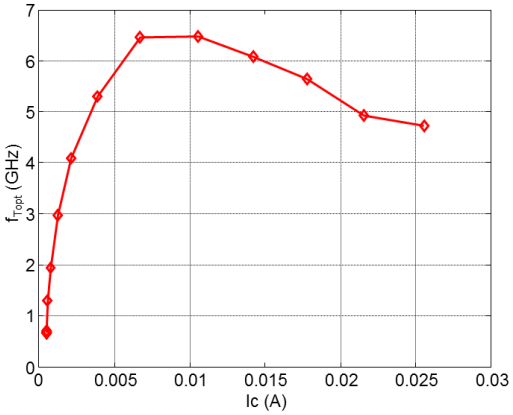

Fig. 11. Optical transition frequency f_{Topt} as a function of the collector current. The injected optical power is 2.38 mW.

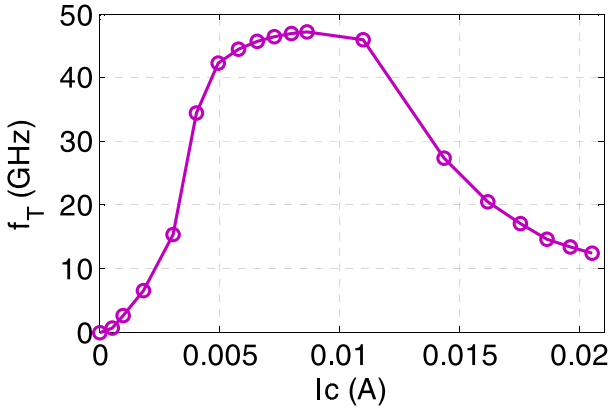

Fig. 12. Electrical transition frequency f_T as a function of the collector current.

2) *Medium Current Region:* The peak of f_{Topt} is reached between $I_C = 6$ and 12 mA. The frequency behavior in this region is mainly limited by the carrier time to reach the metal contacts. Photogenerated carrier transit time is the main limiting factors of the peak f_{Topt}.
3) *High Injection Current Region:* For I_C greater than 12 mA, f_{Topt} quickly drops, due to the injection of a large number of carriers (Kirk effect) in the device which limits the speed of HPTs.

The peak value of f_{Topt} (6.5 GHz) is very small compared to its equivalent electrical transition frequency ($f_T = 47.3$ GHz), as shown in Fig. 12. Unlike f_T, f_{Topt} is influenced by additional terms related to the photodetection mechanism such as additional transit time and junction capacitances introduced by the injected optical power.

The intrinsic parameters of the HPT such as the capacitances and transit time can also be deduced experimentally from optical transition frequency. These parameters could be used in optical system modeling to implement the HPT as a photodetector as well as for future study of the HPT structures. The OM transition time delay τ_{F_OM} is the time required by the OM photogenerated carriers to reach any contact and is calculated from f_{Topt} according to $\tau_{F\_\text{OM}} = 1/(2\pi f_{\text{Topt}})$ [19]. Fig. 13 shows the OM transition delay versus

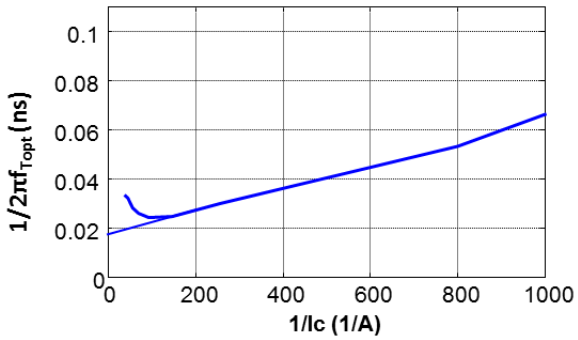

Fig. 13. OM transit time delay versus $1/I_C$ to extract the junction capacitances from the curve slope and the OM transit time from y-intercept.

TABLE I
EXTRACTED JUNCTION CAPACITANCES AND FORWARD TRANSIT TIMES OF THE HPT ILLUMINATED AT THE POSITION CORRESPONDING TO THE OPTIMAL f_{TOPT}

Electrical		**Total (Opto-microwave)**		**Optical**	
C_E(pF)	τ_F(ps)	C_{OM} (pF)	τ_{F_OM} (ps)	C_{opt} (pF)	τ_{F_opt} (ps)
0.798	1.5	1.7	18.7	0.902	17.2

$1/I_C$. The total capacitance (including base–emitter and base–collector depletion, diffusion, and parasitic) and the transit time of the phototransistor can be extracted from the slope and y-intercept of the transition time delay curve, respectively. Table I shows the comparison of the extracted electrical (τ_F and C_E), OM (τ_{F_OM} and C_{OM}), and optical (τ_{F_opt} and C_{opt}) transit times with the related capacitances. The first two parameters (electrical and OM) are extracted from f_T and f_{Topt}, respectively. The optical terms are deduced by removing the electrical terms from the OM ones.

Larger values of capacitance and transit time under OM operation mean that photogenerated carriers cover a longer path than the electrically generated ones. Indeed, the active region of the electrical transistor corresponds to the vertical region of the emitter contact, whereas the transistor effect (active area of the HPT) under OM operation is distributed along the whole device with additional lateral paths of photocarriers to reach the electrical contacts. Similarly, capacitance is larger under OM operation, when compared with under electrical operation, as the active surface of the structure increases related to the photodetection process. This implies that both the junction and diffusion capacitances increase related to the injected optical power.

We deduce the "optical" capacitance and transit time by removing the electrical parameters from the OM ones. These values correspond to the additional capacitance and transit time due to the additional path length and the equivalent active surface area increase encountered by photogenerated carriers compared to the electrical ones. "Optical" capacitance is higher than the half of the total OM one. Such variation of the equivalent capacitance may correspond to its corresponding surface area that is multiplied by a factor of 2 in dimension. Optical transit time is larger than the electrical one. Considering that the vertical stack is unchanged, this may be attributed to a lateral path required for holes to be amplified or for electrons injected from the emitter to reach the photogenerated holes in the base region.

IV. CONCLUSION

This paper considered a SiGe/Si phototransistor developed by using the industrial SiGe HBT technology without modifying the vertical stack of layers. The OM-SNOM analyze is shown to be crucial to understand the behavior of such SiGe HPTs. It allows the extraction of the dc and dynamic behaviors of the device for all the positions of the illuminating optical fiber. As slow carriers from the substrate diode affect the dynamic response of the SiGe/Si HPTs, an extraction method has then been developed to isolate the substrate effect and then deduce the intrinsic behavior of the HPT; an intrinsic optical transition frequency of 6 GHz has been obtained. Thus, the impact of the 2-D carriers flow in the intrinsic phototransistor structure is demonstrated. The speed increases when we illuminate the HPT close to the base contact and it gradually decreases when the optical beam moves away from the base–emitter contact. This is due to the speed of holes which are collected at the base–emitter region.

The internal electrical parameters such as transit time and capacitances of the phototransistor are extracted and can be an input for future modeling of the phototransistor. Further studies using a single-mode optical fiber would be interesting for a more precise modeling of the SiGe HPT and for a reduction of the substrate diode effect when illuminating the optical window.

Several alternatives exist to eliminate the substrate contribution, as the design of metallic diaphragms around the optical window to hide the substrate PD, or through lateral illumination of the HPT. Alternatively, taking advantage of the substrate effect could be envisaged for a combined HPT-PD structure. The influence of the 2-D carriers flow effect can also be avoided or minimized via a proper design of the metal contacts to get a symmetric contact of the collector, base, and emitters that will make the electrical field more vertical.

REFERENCES

[1] C. Viana *et al.*, "Hybrid photo-receiver based on SiGe heterojunction photo-transistor for low-cost 60 GHz intermediate-frequency radio-over-fibre applications," *Electron. Lett.*, vol. 51, no. 8, pp. 640–642, Apr. 2015.

[2] J. Guillory, A. Pizzinat, B. Charbonnier, and C. Algani, "60 GHz intermediate frequency over fiber using a passive multipoint-to-multipoint architecture," in *Proc. IEEE NOC*, Newcastle-Upon-Tyne, U.K., Jul. 2011, pp. 44–47.

[3] K.-H. Lee, J.-Y. Kim, W.-Y. Choi, H. Kamitsuna, M. Ida, and K. Kurishima, "Low-cost optoelectronic self-injection-locked oscillators," *IEEE Photon. Technol. Lett.*, vol. 20, no. 13, pp. 1151–1153, Jul. 1, 2008.

[4] J.-Y. Kim, C.-S. Choi, W.-Y. Choi, H. Kamitsuna, M. Ida, and K. Kurishima, "Characteristics of InP–InGaAs HPT-based optically injection-locked self-oscillating optoelectronic mixers and their influence on radio-over-fiber system performance," *IEEE Photon. Technol. Lett.*, vol. 19, no. 3, pp. 155–157, Feb. 1, 2007.

[5] Y. Zhu, Q. Yang, and Q. Wang, "Resonant cavity SiGe/Si MQW heterojunction phototransistor grown on the SIMOX substrate for 1.3 μm operation," in *Proc. 47th Electron. Compon. Technol. Conf.*, San Jose, CA, USA, May 1997, pp. 1199–1204.
[6] Z. Pei *et al.*, "A high-performance SiGe-Si multiple-quantum-well heterojunction phototransistor," *IEEE Electron. Device Lett.*, vol. 24, no. 10, pp. 643–645, Oct. 2003.
[7] J. L. Polleux, F. Moutier, A. L. Billabert, C. Rumelhard, E. Sonmez, and H. Schumacher, "A strained SiGe layer heterojunction bipolar phototransistor for short-range opto-microwave applications," in *Proc. IEEE MWP*, Budapest, Hungary, Sep. 2003, pp. 113–116.
[8] M. D. Rosales, J. Schiellein, C. Viana, J.-L. Polleux, and C. Algani, "Full area emitter SiGe phototransistor for opto-microwave circuit applications," in *Proc. IEEE 9th Int. Conf. Group IV Photon.*, San Diego, CA, USA, Aug. 2012, pp. 294–296.
[9] Z. Pei *et al.*, "Bandwidth enhancement in an integratable SiGe phototransistor by removal of excess carriers," *IEEE Electron Device Lett.*, vol. 25, no. 5, pp. 286–288, May 2004.
[10] T. Yin, A. M. Pappu, and A. B. Apsel, "Low-cost, high-efficiency, and high-speed SiGe phototransistors in commercial BiCMOS," *IEEE Photon. Technol. Lett.*, vol. 18, no. 1, pp. 55–57, Jan. 1, 2006.
[11] F. Moutier, J. L. Polleux, C. Rumelhard, and H. Schumacher, "Frequency response enhancement of a single strained layer SiGe phototransistor based on physical simulations," in *Proc. EGAAS*, Paris, France, Oct. 2005, pp. 113–116.
[12] J. P. Helme and P. A. Houston, "Analytical modeling of speed response of heterojunction bipolar phototransistors," *J. Lightw. Technol.*, vol. 25, no. 5, pp. 1247–1255, May 2007.
[13] F. Yuan, J.-W. Shi, Z. Pei, and C. W. Liu, "MEXTRAM modeling of Si-SiGe HPTs," *IEEE Trans. Electron Devices*, vol. 51, no. 6, pp. 870–876, Jun. 2004.
[14] Z. G. Tegegne *et al.*, "Substrate diode effect on the performance of silicon germanium phototransistors," in *Proc. IEEE MWP*, Paphos, Cyprus, Oct. 2015, pp. 1–4.
[15] J.-W. Shi *et al.*, "Performance enhancement of high-speed SiGe-based heterojunction phototransistor with substrate terminal," *Appl. Phys. Lett.*, vol. 85, no. 14, pp. 2947–2949, Oct. 2004, dio: 10.1063/1.1799237.
[16] J. L. Polleux, F. Moutier, A. L. Billabert, C. Rumelhard, E. Sönmez, and H. Schumacher, "An SiGe/Si heterojunction phototransistor for opto-microwave applications: Modeling and first experimental results," in *Proc. 11th Symp. GAAS*, Munich, Germany, Oct. 2003, pp. 6–10.
[17] J. Schiellein *et al.*, "Analysis of opto-microwave paths into a InP/InGaAs UTC-HPT," in *Proc. 41st Eur. IEEE Microw. Conf. (EuMC)*, Manchester, U.K., Oct. 2011, pp. 949–952.
[18] Z. G. Tegegne *et al.*, "An 850 nm SiGe/Si HPT with a 4.12 GHz maximum optical transition frequency and 0.805 A/W responsivity," *Int. J. Microw. Wireless Technol.*, vol. 9, no. 1, pp. 17–24, Feb. 2017.
[19] Z. Tegegne, "SiGe/Si microwave photonic devices and interconnects towards silicon-based full optical links," Ph.D. dissertation, Univ. Paris-Est, Champs-sur-Marne, France, May 2016.
[20] J.-L. Polleux, L. Paszkiewicz, A.-L. Billabert, J. Salset, and C. Rumelhard, "Optimization of InP-InGaAs HPT gain: Design of an opto-microwave monolithic amplifier," *IEEE Trans. Microw. Theory Techn.*, vol. 52, no. 3, pp. 871–881, Mar. 2004.

Zerihun Gedeb Tegegne received the master's degree in optical communications and photonic technologies from the Politecnico di Torino, Turin, Italy, in 2012, and the Ph.D. degree in electronics, optoelectronics and systems from the Université Paris-Est, Champs-sur-Marne, France.

He is currently a Researcher with the ESYCOM Laboratory, ESIEE-Paris, Noisy-le-Grand, France. His current research interests include integrated photonics and optoelectronic and microwave photonics systems.

Carlos Viana received the M.S. degree in electrical and computers engineering from the University of Porto, Porto, Portugal, in 2010, and the Ph.D. degree in electronics, optoelectronics and systems from the Université Paris-Est, Champs-sur-Marne, France, in 2014.

Since 2010, he has been a Researcher with the ESYCOM Laboratory, ESIEE-Paris, Noisy-le-Grand, France. His current research interests include optoelectronic device, integration and packaging, and radio-over-fiber technologies.

Jean-Luc Polleux received the DEA degree in electronic and telecommunications from the University of Bordeaux 1, Bordeaux, France, in 1997, and the Ph.D. degree in optomicrowave field from CNAM, Paris, France, in 2001.

He joined the ESYCOM Laboratory, ESIEE-Paris, Noisy-le-Grand, France, as an Associate Professor. His current research interests include microwave-photonics devices, radio-over-fibre systems, integration and packaging, and optomicrowave devices modeling.

Marjorie Grzeskowiak received the M.Sc. and Ph.D. degrees in electronics and in microelectronics engineering from the Université des Sciences et Technologies de Lille, Villeneuve-d'Ascq, France, in 1996 and 1999, respectively.

In 2000, she joined the ESYCOM Laboratory, University of Paris-Est Marne-la-Vallée, Champs-sur-Marne, in France, as an Assistant Professor, where she is involved in the propagation, design of the millimeter wave passive devices, and magnetic coupling.

Elodie Richalot received the master's degree and the Diploma degree in engineering from ENSEEIHT, Toulouse, France, in 1995, and the Ph.D. degree in electronics engineering from INPT, France, in 1998.

Since 1998, she has been with the University of Paris-Est Marne-la-Vallée, Champs-sur-Marne, France, as an Associate Professor and then as a Professor in electronics in 2010. Her current research interests include modeling techniques, electromagnetic compatibility, urban propagation, and millimeter wave transmission lines.